Prediction of jet noise for realistic flow problems using large eddy simulation

Neeraj Sinha and James P. Erwin
Combustion Research and Flow Technology, Inc.
Pipersville, PA 18947 USA
sinha@craft-tech.com, jerwin@craft-tech.com

A systematic procedure is described to predict the noise emissions from realistic aero-propulsive jets. Large Eddy Simulation (LES) is used to compute the jet flowfield and coupled with the Ffowcs Williams and Hawkings (FW-H) equation for far-field noise predictions. A low-dissipation fifth-order upwind biased finite-volume reconstruction procedure is used along with selective fourth order inviscid flux blending. Higher order explicit time integrators are used for enhanced wave propagation. Also, non-contiguous block interfacing is employed to eliminate the traditional limitations of structured grid topologies for complex geometries. For simple jet configurations the LES/FW-H method is validated with University of Mississippi's National Center for Physical Acoustics (NCPA) experimental measurements. Four unique and more realistic applications are then shown. The first is a hot faceted jet with lobed corrugations, followed by an over-expanded military gas turbine engine exhaust with and without chevrons. Then a twin jet impinging on a jet blast deflector is shown, and lastly are two high aspect-ratio nozzles, one with and one without a bevel. The LES/FW-H methodology is shown to produce reasonable agreement with experimental measurements at modest grid resolutions. Details are discussed about the selected example problems highlighting the challenges associated with applying the tools to realistic geometries and jet configurations.

NOMENCLATURE

α	=	Flux blending parameter, [0, 1]
ADI	=	Alternating direction implicit
BBSAN	=	Broadband shock-associated noise
c_0	=	Acoustic speed in undisturbed fluid
dB	=	Decibel, ref. 20 μPa
D_J	=	Jet exit diameter
DNS	=	Direct Numerical Simulation
FW-H	=	Ffowcs Williams and Hawkings
HRLES	=	Hybrid RANS/LES
JBD	=	Jet Blast Deflector
LDDRK	=	Low-dissipation and dispersion Runge-Kutta
LES	=	Large Eddy Simulation
MPI	=	Message passing interface
NBI	=	Non-contiguous block interface
NPR	=	Nozzle pressure ratio, P_{TOT}/P_a
NCPA	=	National Center for Physical Acoustics
OASPL	=	Overall Sound Pressure Level
P_a	=	Ambient pressure
P_J	=	Jet exit static pressure
p'	=	Fluctuating pressure on FW-H surface
RANS	=	Reynolds Averaged Navier Stokes
Re_D	=	Reynolds number based on Jet Exit Diameter, D_J
ρ_0	=	Density of undisturbed fluid
R_J	=	Jet exit radius
SGS	=	Sub-grid scale
SPL	=	Sound Pressure Level (dB, re 20 μPa)
TKE	=	Turbulent Kinetic Energy
$\vec{u}$	=	CFD fluid velocity on permeable FW-H surface

1. INTRODUCTION

Recent progress in the development of

computational aeroacoustic tools has led to remarkable predictions of noise emissions from subsonic and supersonic jets. Researchers are making accurate predictions of the sound field, including not only overall sound levels but spectral content also. Using Large Eddy Simulation (LES) to resolve turbulent scales well into the inertial range, the noise generating mechanisms of complex flowfields can now be routinely computed. Jet noise components such as Mach wave radiation, broadband shock-associated noise (BBSAN), and jet screech are all identifiable with LES when coupled with an integral solution to the Ffowcs Williams and Hawkings (FW-H) equation. Although many codes are numerically mature, they are often only applied to simplistic jet flows (laboratory scale, round, single jet stream, unheated, etc.). Industry and government organizations are in need of tools that can be applied to more complex applications. In this paper we describe a complete methodology for predicting the noise from more realistic flows, and present a variety of results for such problems.

Jet noise sources are challenging to compute numerically for a variety of reasons. LES codes have the capability to predict turbulent statistics accurately given sufficient resolution for a jet Reynolds number, Re_D (based on jet exit diameter, D_J). For full scale jets, high Re_D can prove very restrictive due to increased grid resolution requirements and limited computational resources. In three-dimensions, the number of grid points required scales as $Re^{9/4}$ and the computational cost scales as Re^3 [1]. The dissipative scales at large Re_D need to be modeled with some form of sub-grid scale (SGS) model and much work has been focused on the proper way to model these scales with regards to jet noise (a comprehensive review is given by Bodony and Lele [2]). With the exception of Shur *et al.* [3], all Re_D considered are below 500,000. The Reynolds numbers for full scale jet engine exhausts are often an order of magnitude higher than what is commonly reported in the literature. LES codes still require further validation at these higher Re_D. However, great challenges exist in obtaining experimental measurements of the jet exhaust for full scale, hot engines. Until these measurements are performed and made available to validate full scale LES calculations, confidence in the codes is gained by performing validations at laboratory scale.

Another important consideration when predicting jet noise using LES is the inflow (nozzle exit) boundary condition. In question is the dependency of the shear layer growth, potential core length, and ultimately far-field noise amplitude and directivity on the initial boundary layer thickness and turbulence characteristics. Many researchers have directed attention towards the prescription of turbulent fluctuations at the nozzle lip in order to encourage proper turbulent transition and shear layer growth [6–7]. Although certain methods can be tuned to match experimental measurements of laboratory jets, realistic jets that contain three-dimensional geometries and internal nozzle features can not be treated with these methods. There ultimately exists a need to compute the internal nozzle flow directly and describe LES inflow boundary conditions based on the specific application. In this paper, all of the inflow boundaries for the LES are obtained from either a pre-cursor RANS simulation of the internal nozzle, or a simultaneous RANS/LES calculation that solves the internal nozzle flow simultaneously with the LES. The SGS model at the RANS/LES interface is informed from the RANS model inside the nozzle. The LES inflow boundary condition is therefore more accurately defined than assuming boundary layer thickness, shape, and turbulent characteristics. Shur *et al.* similarly describe a "two-step RANS-LES" approach which uses precursor RANS calculations as inflow boundary conditions for LES [3]. Clearly, the use of artificial inflow forcing can excite the jet and add unwanted noise sources if not performed carefully. Therefore, in this work, no artificial forcing methods have been employed.

The focus of the current work is to demonstrate the practical application of the LES/FW-H method towards realistic problems. Previous applications of the method by the authors have been limited to mostly free-jets with round nozzle topologies [8–10] and more recently twin-nozzle and vertically impinging jet configurations [10–11]. In this paper, more detailed cases are described including noise reduction devices and installation effects. Code enhancements are also discussed that allow for the calculation of these realistic configurations. The remainder of the paper is organized as follows. The computational methodology is summarized including specific features of the LES code that aid in computing realistic jet noise problems. Various validation cases are then shown, all using experimental data acquired at University of Mississippi's National Center for Physical Acoustics (NCPA). Four realistic jet noise applications then are described in detail, including two noise reduction devices, a twin-jet exhausting over a ground plane and impinging on a jet blast deflector, and lastly a rectangular nozzle configuration. Finally, conclusions are given regarding the current status of the methodology and future work is recommended.

2. COMPUTATIONAL METHODOLOGY

2.1. CRAFT CFD® LES CODE

For the LES calculations we use a structured grid Navier Stokes solver, CRAFT CFD®, which has been used extensively for the evaluation of jet noise reduction concepts for military gas turbine engines [8]. A low-dissipation fifth-order upwind biased finite-volume reconstruction procedure is used with Roe's shock capturing, approximate Reimann solver [12]. Local dissipation is added near sharp flow gradients as needed, otherwise stability is achieved through a combination of the upwind scheme dissipation and selected SGS eddy-viscosity model. A DNS study of subsonic and supersonic turbulent free shear flow has demonstrated the capability of the fifth-order reconstruction scheme [13].

Although every problem has unique attributes regarding boundary conditions, some common procedures are shared among them. High-order acoustic radiation boundary conditions that have been developed with success for academic problems [14–15] are not used in the far-field. These types of boundary conditions tend to be more complicated to implement in production codes and also assume some global features of the flowfield, such as a mean flow direction and source location. Instead, grid stretching is performed and the flux calculations are reduced to first-order to dampen outgoing waves and minimize reflections from boundaries. It is found that this method is the most robust when applied across the range of problems encountered to date. Upstream of the nozzle exit, the grid is extended and stretched with care to ensure that the subsonic inflow boundary condition does not interact with the jet and cause unphysical instabilities. At the outflow, an extrapolation or subsonic back pressure is enforced depending on the local flow characteristics.

Various simulation options are available in CRAFT CFD® with regards to SGS modeling and RANS/LES interfacing. RANS calculations are carried out with a highly validated k-ε two equation turbulence model that supports variable turbulent Prandtl/Schmidt number capabilities [16–17]. Blending between RANS and LES regions has traditionally been performed using either a zonal method or an innovative Hybrid RANS/LES (HRLES) methodology, originally developed for subsonic cavity flows [18]. In zonal RANS/LES, the RANS region is pre-computed and the solution at the RANS/LES interface is enforced as a steady boundary condition for the LES. This method is applicable when the RANS regions are not expected to be influenced by the unsteadiness in the LES region, and when the regions themselves are well-defined and stationary. For realistic applications where the RANS and LES regions are not well-defined and have the potential to influence one another, a softer blending method must be employed. The HRLES method has proven effective with sufficient grid resolution for certain cases. However, often times the eddy-viscosity delays turbulence transition close to the nozzle lip and alters the noise significantly. Unless the boundary layer resolution inside the nozzle of a HRLES calculation is extremely fine, there is no resolved turbulence at the RANS/LES interface and the LES inflow is steady and suffers from the same turbulence transition as the zonal RANS/LES interface procedure. A more promising approach recently implemented is a Delayed Detached Eddy Simulation method (DDES) [19–21], where the characteristic length scale of the turbulence model is derived from the local grid resolution. The specific implementation of the DDES model in CRAFT CFD® is given by Rodebaugh *et al.* [22] and aims to rapidly reduce the turbulent viscosity in the LES region. In LES mode, a one-equation *k*-SGS model is used.

Relatively new to CRAFT CFD® are improvements to the numerical discretization and various explicit time integrators including a four stage, low-dissipation and low-dispersion Runge Kutta (LDDRK) scheme. At any location in the flowfield, the inviscid flux can be defined as a blend of a fourth-order central and fifth-order upwind reconstruction [3–5]. The total flux is the weighted sum of two separate flux calculations, and the weighting parameter is dynamically chosen based on local flowfield features. The inviscid flux is given by

$$F(x,t) = \alpha(x,t)F_4(x,t) + \left(1-\alpha(x,t)\right) + \left(1-\alpha(x,t)\right)\, F_5(x,t) \qquad (1)$$

where $F(x,t)$ is the total flux, F_4 is the fourth-order central flux and F_5 is the fifth-order upwind flux. The weighting parameter $\alpha(x,t)$ varies between 0 and 1 based on the local flow conditions. In areas of high eddy-viscosity or linear wave propagation, the flux weighting is mostly central ($\alpha \sim 0.7$) where around shocks or in coarsely resolved RANS regions, the flux is given primarily an upwind weighting ($\alpha \sim 0.01$). In addition to second-order implicit time integration based on Alternating direction implicit (ADI) factorization, there are various flavors of Runge-Kutta explicit integrators including a four-stage LDDRK with weights defined from Hu *et al.* [23]. The LDDRK scheme is as computationally expensive as approximately two or three sub-iterations using the second-order ADI scheme. When possible all of the simulations are carried out using LDDRK for improved wave propagation, but sometimes the boundary layer resolution requirements demand an unrealistically small time step when using LDDRK relative to the ADI scheme.

2.2. NON-CONTIGUOUS BLOCK INTERFACING (NBI)

Structured grids can become very restrictive when performing LES for complex geometries. Using contiguous block interfaces, the structured grid topology and resolution in the LES region needs to be kept throughout the entire block. Without careful grid construction, significant amounts of grid can be wasted in regions far away from the LES region. In addition, the grid topology required to fit a noise reduction concept at the nozzle lip with a body-fitted grid is often too complicated to continue throughout the entire domain.

To remedy this limitation of structured grids, Non-contiguous Block Interfacing (NBI) has been implemented in many simulations. The block interfaces no longer need to maintain consistent topologies or resolution and away from regions of interest, the grid is coarsened towards the freestream boundaries. This type of block interfacing is similar to a Chimera or overset grid approach, where the boundary faces are not abutting and acquire their boundary condition through an interpolation of neighboring information [24] . The finite volume flux for an NBI cell in the current code is computed from a weighted contribution of its surrounding cells. A validation case is shown in Figure 1 and Figure 2. A non-contiguous grid topology in two dimensions is shown in Figure 1 where the grid is refined by a factor of 2:1 along the bottom of the domain. A solid reflective wall boundary condition is enforced along the bottom edge of the finer domain. A Gaussian pressure and density distribution is shown propagating in time in Figure 2 at three instances in time. The pulse is originated only a few dimensionless units above the NBI. As seen in the figure, the pulse propagates through the NBI and no spurious reflections are generated by the interface.

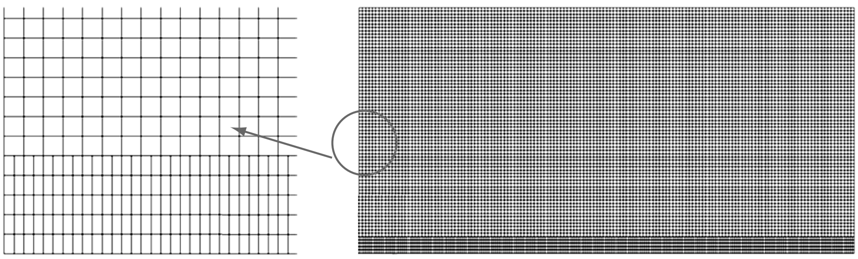

Figure 1: *Validation case for NBI.*

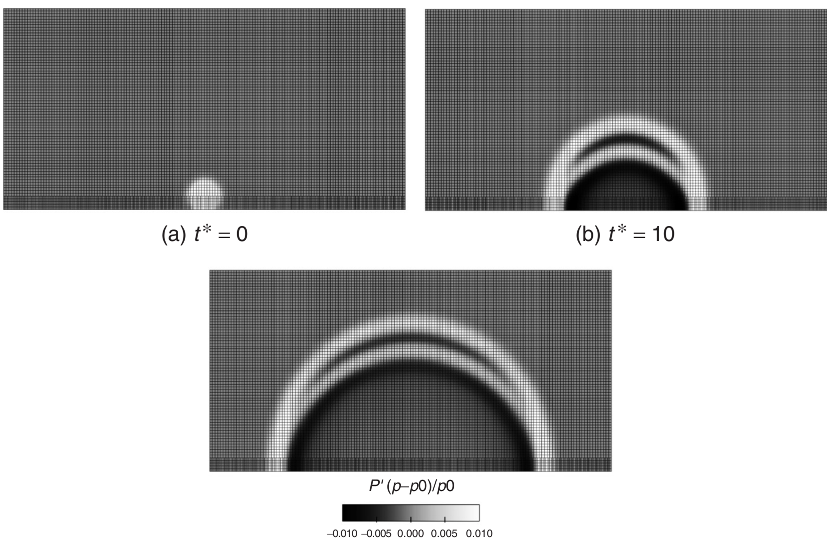

(a) $t^* = 0$ (b) $t^* = 10$ (c) $t^* = 20$

Figure 2: *Propagation of Gaussian pulse at three non-dimensional times t* = t/dt.*

2.3. CRAFT FW-H FAR-FIELD ACOUSTIC SOLVER

The acoustic signatures at far-field microphone locations are calculated through a transformation of the near-field LES solution. The transformation solves the FW-H equation using Farassat's Formulation 1A [25]. The FW-H equation is an exact rearrangement of the continuity and Navier Stokes equations into an inhomogeneous wave equation. An in-depth analysis of the FW-H method and an alternately useful form of Formulation 1A is given by Brentner and Farassat [26]. The solver is highly parallelized using Message Passing Interface (MPI) and can compute the noise for many microphone locations (observers), far exceeding the number of microphones possible in an experimental array.

During the LES, acoustic variables are stored on a fictitious "permeable" data surface surrounding the jet. Consider the example in Figure 3, where a FW-H surface is shown surrounding the shear layer of a full scale, military gas turbine engine exhaust. The instantaneous pressure field is shown in grayscale overlaid with colored vorticity contours. A common practice is to place the data surface (shown as dashed red lines) just outside of the highest vorticity in the shear layer. The goal of the FW-H surface placement is to be as tight to the shear layer as possible, to avoid numerical dissipation due to grid stretching, while not intersecting high shear layer non-linearities. In all of the cases described in this paper, no "end-cap" is used on the FW-H surface and vortical structures exit the domain without intersecting the surface. At the majority of angles to the jet axis, the noise predictions are relatively unaffected by the presence of this surface if the LES extends sufficiently downstream. Delicate balances exist between the tightness of the FW-H surface to the jet shear layer and how much non-linearity is permitted to intersect the FW-H surface. Aiding any abuses of this grey area is an alternative formulation of the integral solution [29], where the density at every differential area on the FW-H surface is computed as $\rho = \rho_0 + p'/c_0^2$, where ρ_0 and c_0 are the density and sound speed in the undisturbed flow, respectively, and p' is the fluctuating pressure. An added benefit of this formulation is the requirement to store only four solution variables on the surface (p, $\vec{u}$) instead of five. The far-field noise is then computed at any observer location as a post-processing step, and these observer locations do not need to be defined before the LES begins. Lyrintzis performs a comprehensive review of a variety of methods for evaluating far-field acoustic signals from CFD [30].

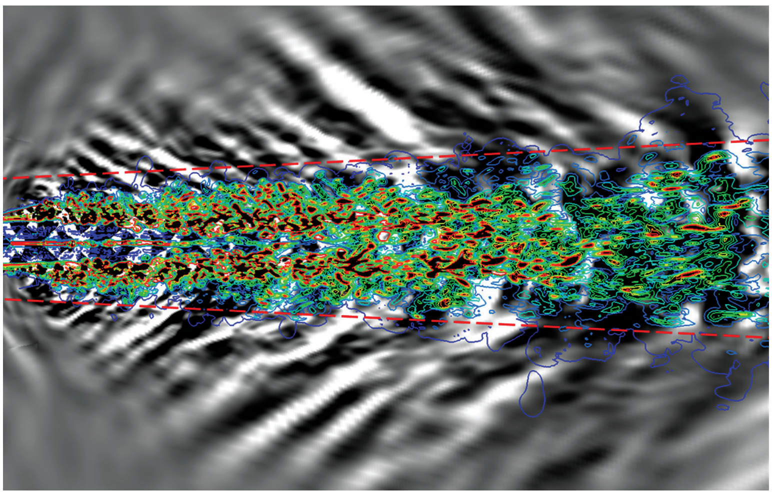

Figure 3: Example of FW-H surface enclosing a supersonic free-jet.

2.4. CODE SCALABILITY

For full scale, realistic applications of LES for noise predictions, the computational grid becomes quite large. In order for codes to solve such flowfields, they must be properly parallelized and demonstrate the ability to scale with increasing number of processors. Figure 4 shows the efficiency and speedup of a CRAFT CFD® five-equation LES case over a wide range of processors for a 30 million cell grid. The scalability study was performed on a Cray XT5 system with a baseline of 42 minimum processors. The grid consisted of 28 blocks and all boundaries were contiguous. Better than ideal speedup and efficiency is achieved using approximately 1000 processors. This is due to the ability of the domain decomposition to be better load balanced when using more processors. On the same system, a 128 million cell grid is solved with up to 1958 processors, as shown in Figure 5 using 299 processors as a baseline. This case was run with the seven-equation HRLES code option and consisted of 117 blocks. Again the code is shown to scale very well.

3. LABORATORY JET SIMULATIONS OF NCPA EXPERIMENTAL CONFIGURATIONS

In the previous few years, the LES/FW-H system has been thoroughly tested on multiple datasets experimentally acquired by Dr. Jack Seiner and his colleagues at NCPA. Without working closely with Jack and his experimental

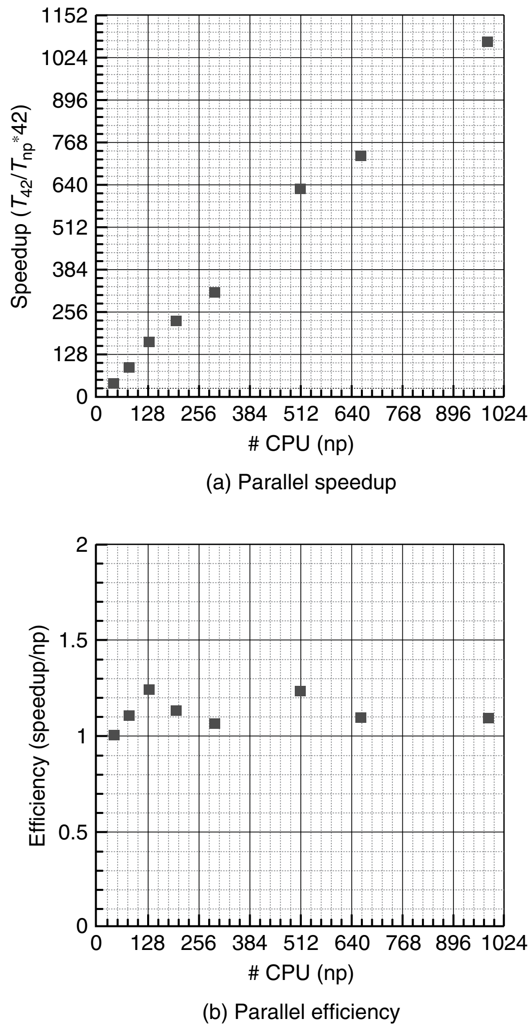

Figure 4: Scalability of CRAFT CFD® code using 30 M cells on a Cray XT5 system (a) Parallel speedup (b) Parallel efficiency.

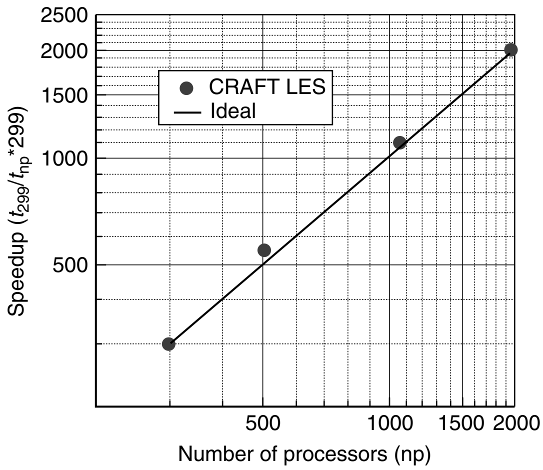

Figure 5: Scalability of CRAFT CFD® code using 128 M cells on Cray XT5 System.

data throughout the development phases, these tools would not be as mature and robust as they are today. In this section we describe just a few of these cases including cold, heated, and twin-jet configurations.

3.1. UNDER-EXPLANDED MACH 2, COLD LABORATORY JET

One of the first validation studies performed is an under-expanded (P_J/P_a = 1.47), cold laboratory jet based on the well-known experiments of Seiner [27]. The computational grid is a very modest 2.5 million cells, and hyperbolic tangent velocity and density profiles are imposed at the nozzle exit [28]. Figure 6 shows time averaged Mach number and instantaneous LES temperature for the jet, and Figure 7 shows the time-averaged centerline Mach number and pressure compared with the Seiner experiments. The time-averaged LES captures the shock cell strengths and spacing for this jet quite well given the relatively low grid resolution.

3.2. OVER-EXPANDED MACH 1.5, HOT LABORATORY JET

This supersonic jet represents a 1/10th scale over-expanded Mach 1.553 faceted laboratory nozzle, operated at conditions comparable to tactical take-off [8]. The nozzle exit profile consists

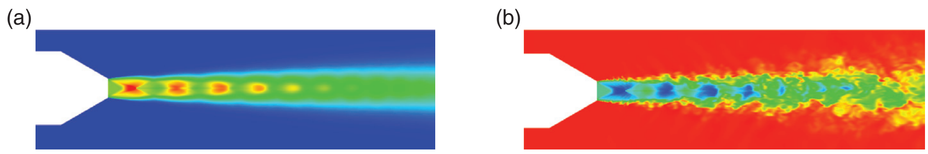

Figure 6: LES solution for Seiner under-expanded jet (a) Time-averaged Mach number and (b) Instantaneous Temperature.

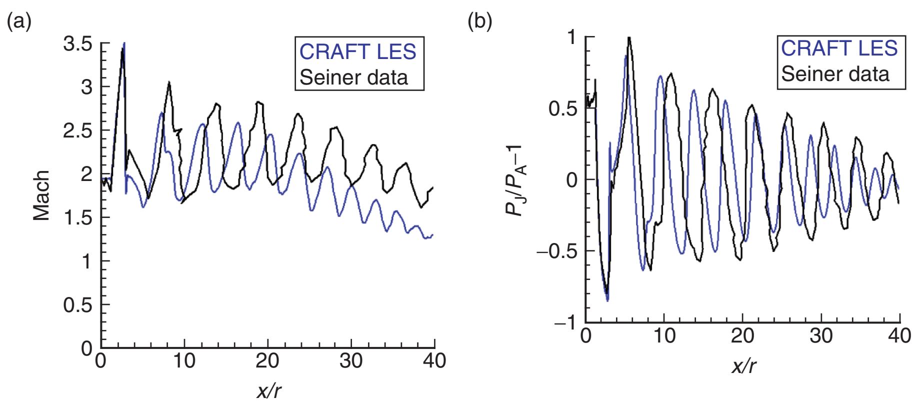

Figure 7: Time-averaged LES compared with experiment along centerline for seiner under-expanded jet (a) Mach number and (b) Pressure.

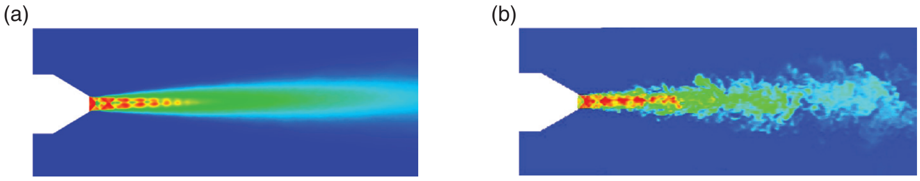

Figure 8: LES solution for Over-expanded Hot Jet (a) Time-averaged Mach number and (b) Instantaneous Temperature.

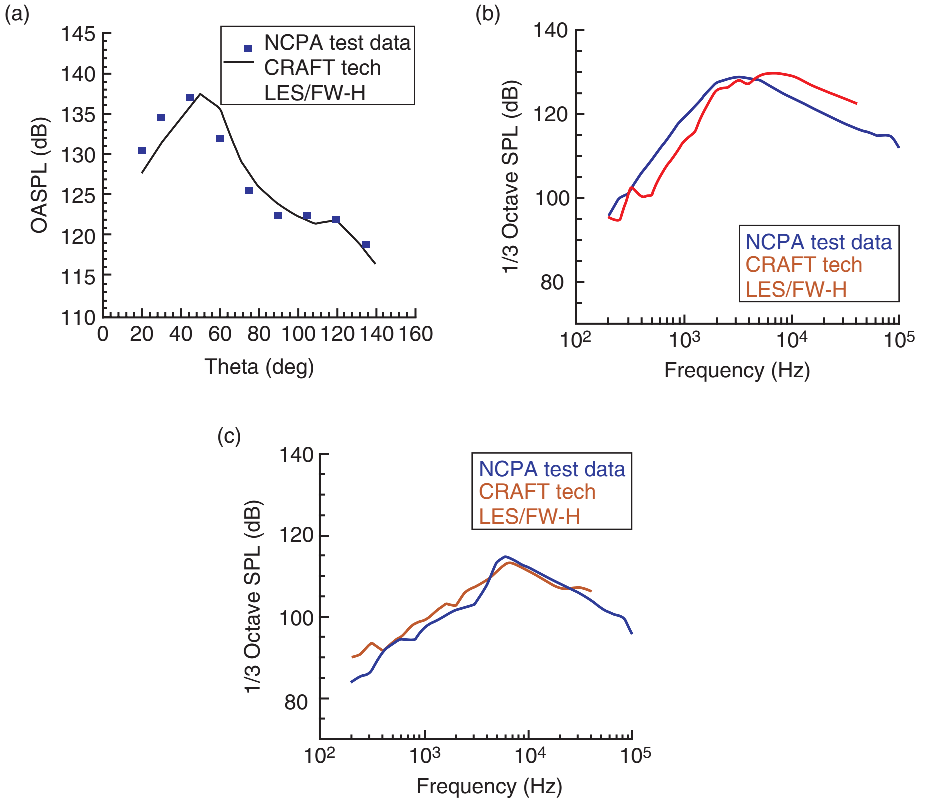

Figure 9: LES/FW-H predictions of over-expanded hot jet compared with NCPA test data (a) OASPL and 1/3 Octave SPL in (b) Downstream and (c) Upstream directions.

of twelve facets of equal length, namely a regular dodecagon. The nozzle exit conditions from a RANS solution were imposed as boundary conditions for the LES simulation of the jet. The computational grid is approximately five million cells. Figure 8 are time-averaged Mach number and instantaneous temperature solution contours for the jet. The far-field noise predictions using the LES/FW-H method are shown in Figure 9 compared with experimental measurements at NCPA. Reasonable agreement with NCPA is achieved not only for OASPL but also the 1/3 Octave SPL in both the downstream and upstream directions. The broadband shock noise component in the upstream direction is captured around 5–6 kHz and a level OASPL profile in the upstream direction is seen between 80 and 120 degrees, associated with a shock-containing jet.

3.3. TWIN OVER-EXPANDED MACH 1.5, HOT LABORATORY JETS

The same over-expanded hot jet was used in a twin-jet configuration for further validation with NCPA test data. Figure 10 is a picture of the twin jet in the NCPA anechoic room and Figure 11 is the twin O-H grid topology used for the LES at the nozzle exit plane, which consisted of nine million cells. Time-averaged and instantaneous Mach number solutions from the LES are

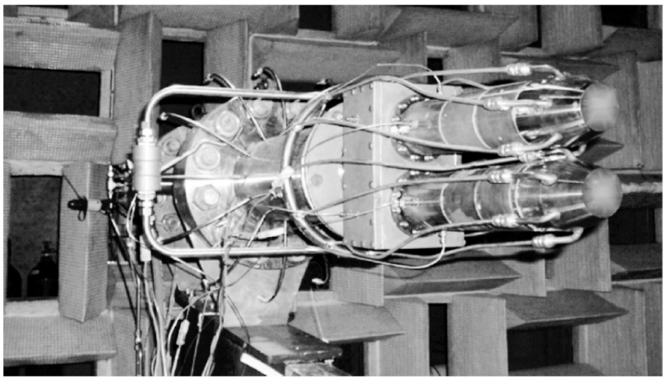

Figure 10: Experimental twin-jet setup at NCPA.

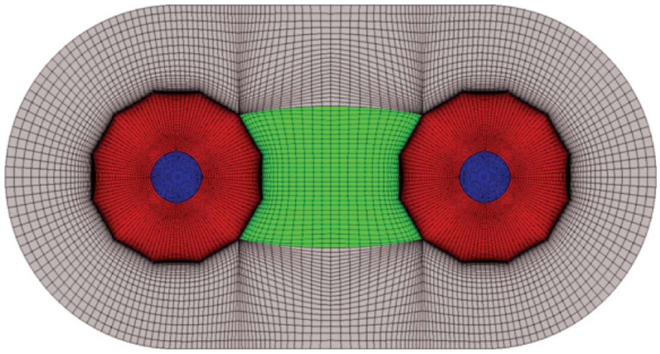

Figure 11: Twin O-H LES grid topology.

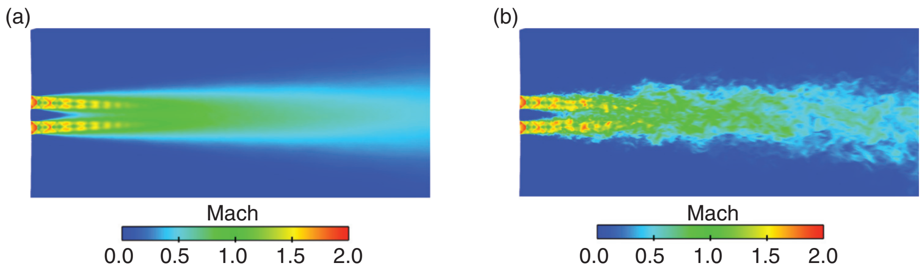

Figure 12: LES Mach number contours for twin-jet (top view) (a) Time-averaged and (b) Instantaneous.

shown as a top view in Figure 12, highlighting the complexity of the flowfield and the twin-jet interaction. LES/FW-H noise predictions are compared with NCPA measurements at 55 D_J in Figure 13. The OASPL in both the side-line and transverse direction (under flight path) agree well. Also, the narrow band spectra in the downstream and upstream directions have similar amplitudes and shape. The LES captured a screech tone and also BBSAN in the upstream direction.

4. REALISTIC JET NOISE APPLICATIONS

The LES/FW-H methodology has been validated for a variety of single stream jets operating over a range of conditions and also a heated twin-jet. The next step forward towards using these tools to guide future aerospace design is applying them to more complex problems and testing their utility. Described here are four unique and challenging jet noise problems. The first is a hot faceted jet with lobed corrugations, followed by an over-expanded military gas turbine engine exhaust with and without chevrons. Then a twin jet impinging on a jet blast deflector is shown, and lastly are two high aspect-ratio nozzles, one with and one without a bevel.

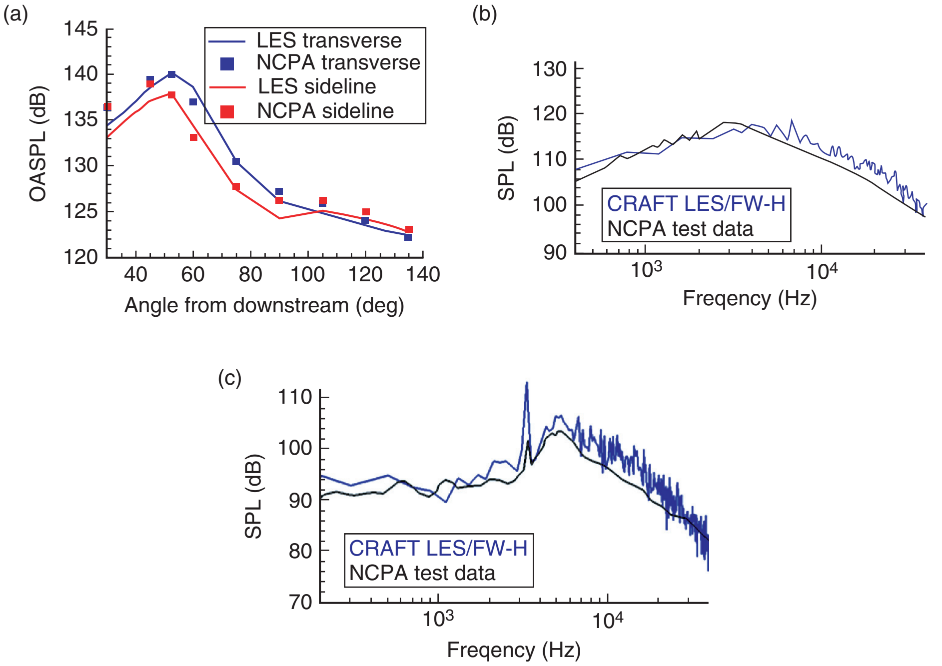

Figure 13: LES/FW-H predictions of twin over-expanded hot jet compared with NCPA test data (a) OASPL and narrowband SPL in (b) Downstream and (c) Upstream directions.

4.1. HOT, OVER-EXPANDED JET WITH NCPA LOBE CORRUGATION CONCEPT

A research project led by University of Mississippi's NCPA involved the design and optimization of corrugated nozzle inserts. The design optimization focused on maintaining or improving thrust while reducing noise emissions. The approach is to replace the flat faceted seal in the engine nozzle with corrugated concepts (shown in Figure 14). These corrugated seal concepts are also referred to as lobes or lobed nozzles. Pre-test thrust predictions were performed for a baseline Mach 1.553 12-faceted nozzle, a 12-lobe NCPA nozzle, an advanced 12-lobe NCPA nozzle, and a lobe concept developed by CRAFT Tech. Refer to Section 3.2 for CRAFT Tech's initial noise calculations for the baseline faceted nozzle. Cold flow simulations were performed on multiple nozzle configurations of various area ratios in flows of different nominal pressure ratios. A part of the program was to perform high-resolution LES and far-field noise predictions for the various lobed configurations. In this section, the LES and noise predictions for the CRAFT Tech optimized lobe is shown.

The grid topology used for the CRAFT Tech lobe is shown in Figure 15 and Figure 16. NBI can be seen in both figures and are used to reduce grid resolution in the far-field of the jet. The resolution is greatly increased in the exhaust region but not carried away from the jet where the grid would be wasted. The total cell count for the LES grid is around 56 million, and the flow

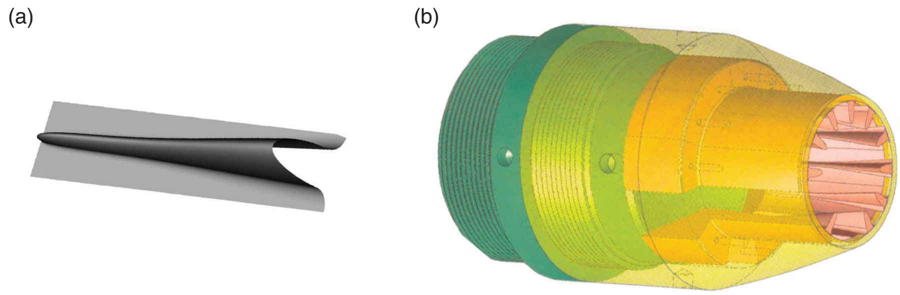

Figure 14: (a) Corrugated Flap Seal and (b) Solid Model with Seals.

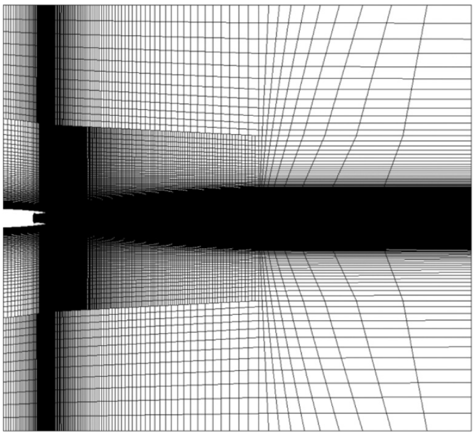

Figure 15: Side view of CRAFT-Tech lobe LES grid topology.

was solved on a Cray XT5 cluster using around 700 processors. The inner nozzle and LES solution were simultaneously solved with the HRLES option in the code.

For this case the jet operates over-expanded at a nozzle pressure ratio of 3.92 and total jet temperature of 1389 degrees Fahrenheit. Instantaneous Mach number contours and resolved turbulent kinetic energy (TKE) are shown in Figure 17. 1/3 Octave SPL predictions for this jet compared with the NCPA measurements are shown in Figure 18 for the upstream and downstream directions. The results are all shown scaled to full-scale frequencies. At 45 degrees upstream, very good agreement is found between the LES/FW-H predictions and the experiment. There is some scatter in the lower frequencies of the LES/FW-H predictions due to the finite sampling time. However, the slope up to the BBSAN peak around 600 Hz agrees very well, and the peak SPL agrees within 1–2 dB at this location. In the downstream direction of 135 degrees, the peak in the spectra agrees fairly well with the measurements. Below the peak frequency the predictions are between 2–4 dB lower than the experiment and above the peak frequency the predictions are between 2–4 dB higher before the grid cut-off of around 5 kHz. A more comprehensive comparison of the noise field is shown in Figure 19 where contours of 1/3 Octave spectra are shown at all angles to the jet. On the x-axis is the log of frequency, and the y-axis is angle to the jet (from upstream). At the bottom of the figures are upstream angles and the top are downstream angles. An over-all good agreement is seen in SPL and directivity shape of the two jets. At angles below 100 degrees the predictions are higher than the measurements above the BBSAN peak. Also, a slight difference in peak

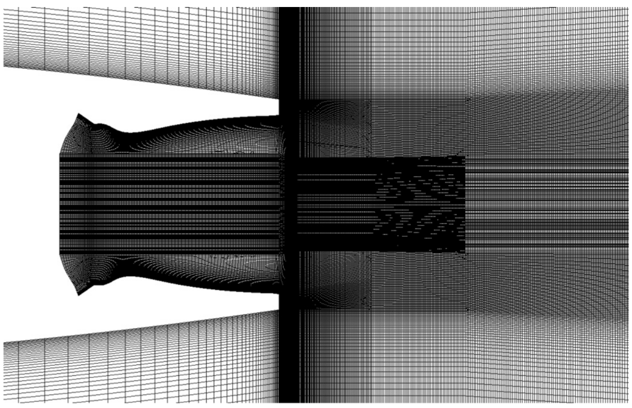

Figure 16: Zoomed-in side view of CRAFT Tech lobe LES grid topology, showing inner nozzle connected to LES domain.

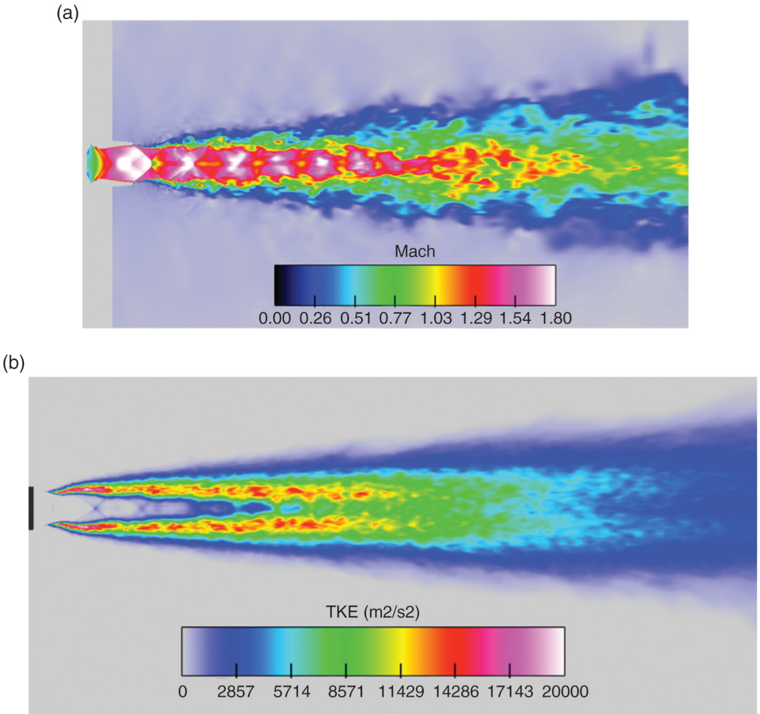

Figure 17: LES solution for CRAFT Tech lobed jet (a) Instantaneous Mach number (b) Resolved TKE.

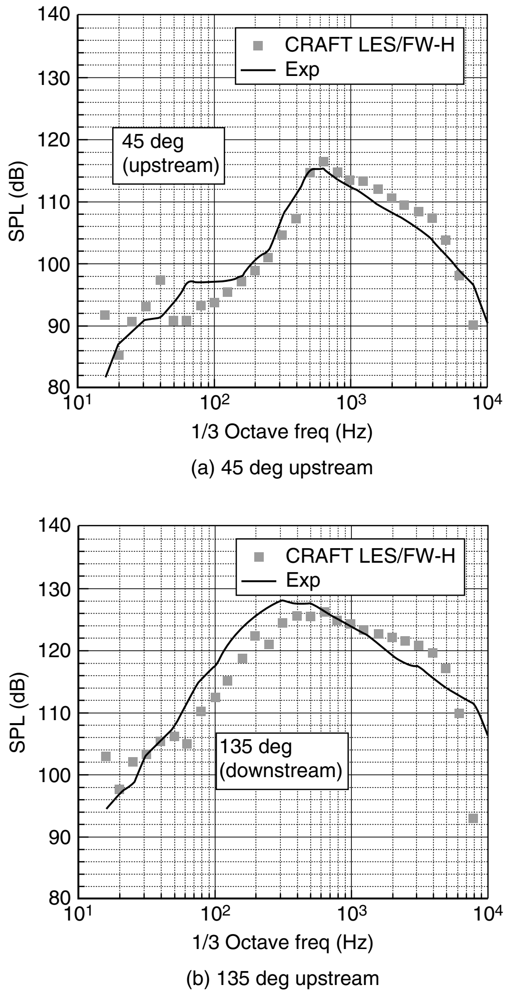

Figure 18: Comparison of NCPA measured noise for Style B with CRAFT Tech LES/FW-H predictions (a) Upstream and (b) Downstream direction.

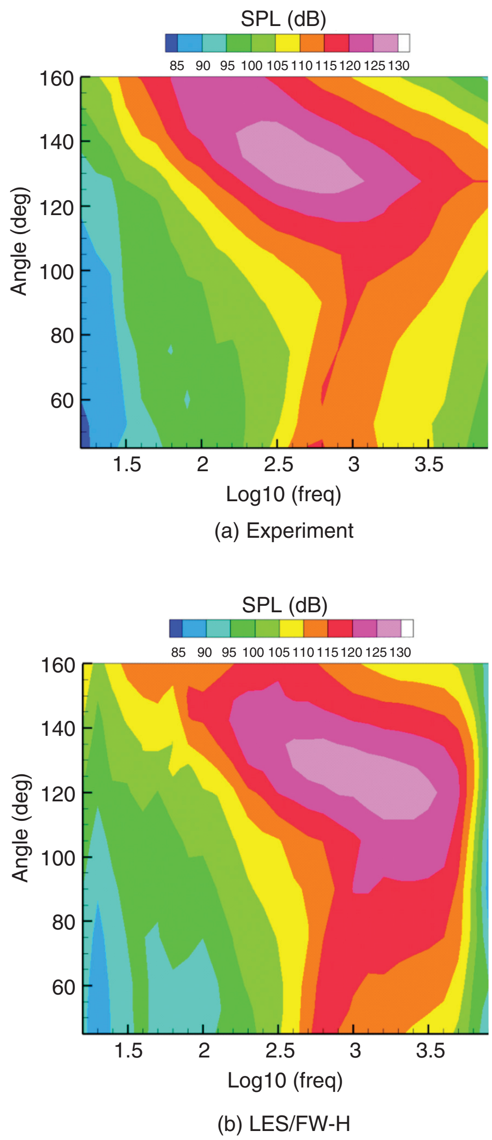

Figure 19: Noise contours for CRAFT Tech lobe (a) NCPA Experiment (b) CRAFT Tech LES/FW-H.

directivity angle can be seen in the figure, which is possibly due to the numerical and experimental jets operating at slightly different settings. This application has shown the capability of the LES/FW-H method to predict the noise for a hot faceted jet with a noise reducing corrugation concept.

4.2. HOT, OVER-EXPANDED FACETED JET WITH CHEVRONS

Noise emissions of a hot, supersonic jet at laboratory scale are predicted with and without a noise reducing chevron concept. The hot jet is representative of an over-expanded, low bypass ratio military gas turbine engine exhaust. Twelve chevrons are added that are non-penetrating, equilateral triangles and extend tangentially to the flow from the nozzle trailing edge. NBI is used not only to increase efficiency of grid resolution but also in a grid topology that allows for the baseline (no chevron) and chevron case to be solved on an identical grid. To activate the chevrons, a boundary condition switch is changed from inter-block communication to a wall boundary condition, representing the infinitely thin chevron blockage. In this method, the inter-block communication boundaries that were previously used for the baseline jet are changed to wall boundary conditions representing the chevron geometries. The calculations were performed with the HRLES option in the code [18]

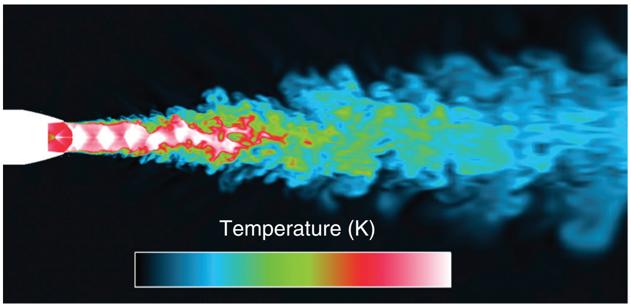

Figure 20: Instantaneous LES Temperature (Baseline).

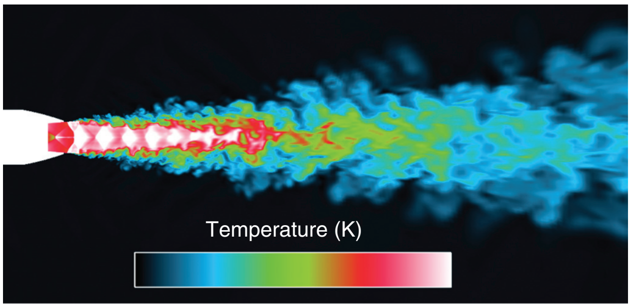

Figure 21: Instantaneous LES Temperature (Chevrons).

using both 5.5 million and 128 million cell resolutions.

Figure 20 and Figure 21 are instantaneous snapshots of temperature for the baseline and chevron case using the 5.5 million cell grid, respectively. There is a time-varying flapping of the shock cell centerline alignment in the baseline case starting at approximately the third cell downstream, whereas the chevrons tend to align the shock cells. The shock cell structure in the baseline case contains a combination of azimuthal and flapping modes, while the chevron jet has a much more stationary core region. Figure 22 and Figure 23 are isometric views of the temperature field for the two cases. The

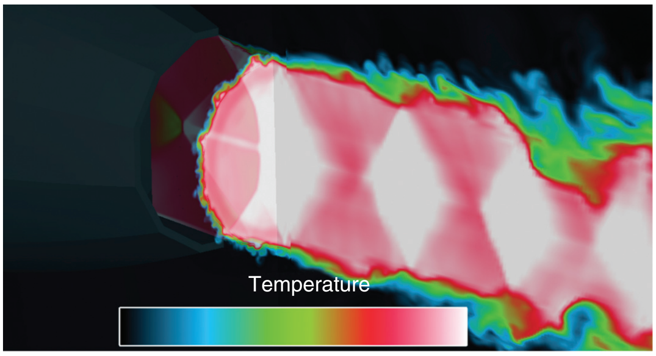

Figure 22: Instantaneous LES Temperature (Baseline).

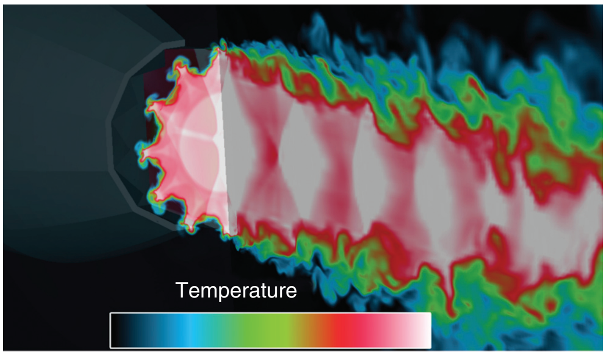

Figure 23: Instantaneous LES Temperature (Chevrons).

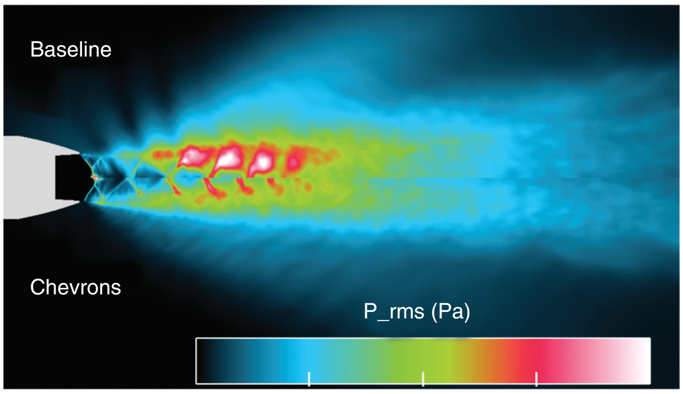

Figure 24: RMS Pressure (Baseline vs Chevrons).

axial cut is located at one jet radius downstream. Even for the baseline case, there is a significant amount of shear layer turbulence resolved at this location. The axial cut of the chevron jet shows a substantial penetration of the entrained flow into the shear layer, due to the pressure imbalance at the nozzle exit. Because the pressure at the nozzle exit is lower than ambient pressure, the entrained flow is pulled through the chevron valley quite strongly.

The RMS pressure contours in Figure 24 indicate that the chevrons may have a significant impact on noise reduction. The peak levels for the baseline jet are much higher than the chevron jet. The high spikes along the outer edge of the core for the baseline case are due to the shock cell motion discussed earlier. This phenomenon was similarly found by Nichols *et al.* [31] when performing high resolution LES of rectangular Mach 1.4 jets. Nichols observed that the peak RMS levels were located along the shear layer region when the jets were flapping and more centralized for non-flapping jets.

Shown in Figure 25 are OASPL predictions for the baseline and chevron jet for observers located on a circular arc approximately 100 D_J from the nozzle exit. The downstream direction is zero degrees and the upstream direction is 180 degrees. The chevrons appear to reduce the downstream noise by as much as 3–4 dB and the noise in the transverse direction a fairly uniform 1 dB. In Figure 26 are 1/3 Octave spectra in the upstream, transverse, and downstream directions, highlighting the noise reduction across a wide range of frequencies in all directions. A BBSAN peak occurs in the upstream direction around 8–9 kHz for both jets. In the upstream direction the reduction is most notably below the BBSAN peak, potentially due to the reduction of a low jet flapping mode. After the BBSAN peak the levels are quite similar. In the transverse direction, the noise reduction can start to be seen above the BBSAN

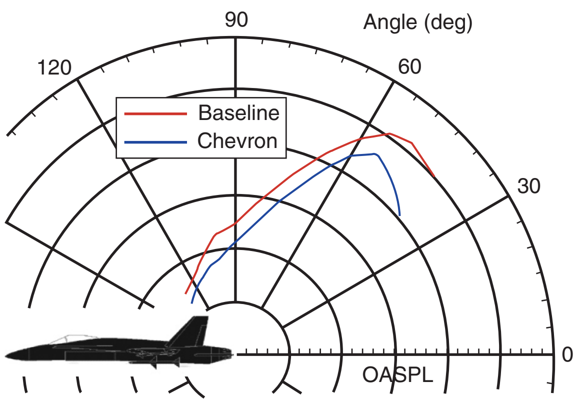

Figure 25: OASPL directivity for laboratory scale hot military gas turbine engine with and without Chevrons.

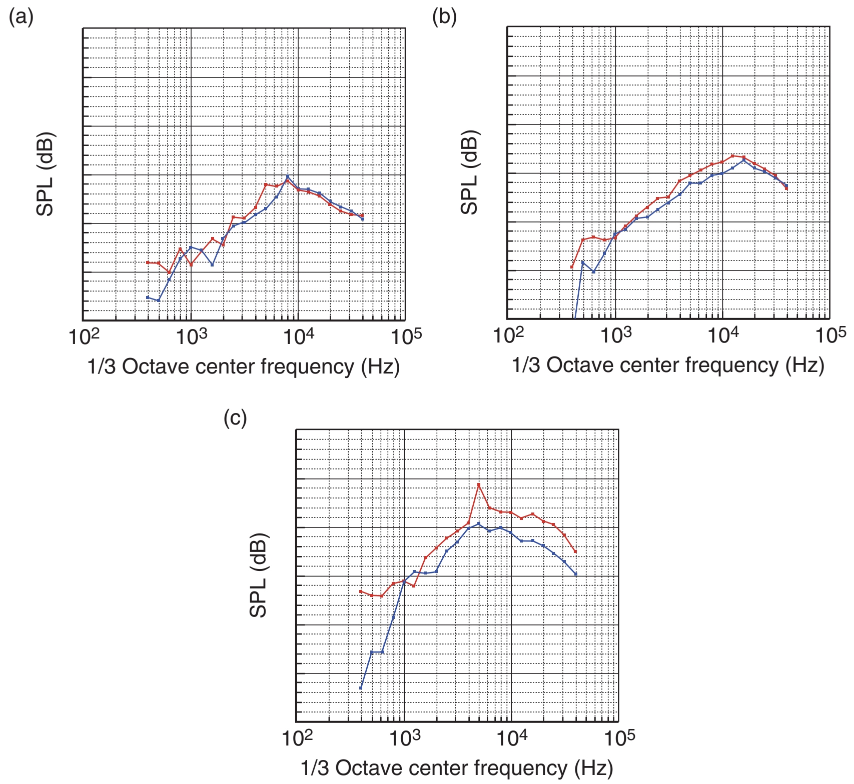

Figure 26: 1/3 Octave SPL spectra for hot military gas turbine engine with and without Chevrons (a) Upstream (115 deg) (b) Transverse (90 deg) (c) Downstream (40 deg).

peak. With the chevrons there is significant reduction of broadband noise in the downstream direction, as well as elimination of the screech tone that was predicted for the baseline case at approximately 4.5 kHz. This tone is attributed to the intense flapping of the shock cells and their interaction with the shear layer. Many differences in the noise between the baseline and chevron jet were identified, but noise reduction devices most likely influence the strength and growth of small scale turbulence, and requires increasingly fine LES grid resolution to capture their impact on the flowfield. A high resolution (HR) calculation consisting of 128 million grid cells will now be shown. The solution from the lower resolution (LR) chevron case was transferred to the HR grid for the flow initialization. Instantaneous LES contours of temperature for the HR and LR case are shown in Figure 27. Many more fine scale features can be seen in the HR calculation, as expected. Also of interest is the additional unsteadiness resolved by the HR calculation in the core. Structures can be seen shedding off the centerline of the shock cells. Although the overall penetration depth of the entrained flow in the HR case is similar to the LR case, the finer scales are better resolved which directly impact the high frequency noise predictions. The HR simulation required approximately two weeks of continuous simulation time using 1958 processors.

A comparison of the instantaneous pressure field for both resolutions is shown in Figure 28. Higher wave number content can be seen throughout the entire shear layer region and around the shocks in the HR calculation. Pressure RMS contours are shown in Figure 29 for both resolutions. The HR calculation has more distinct high RMS regions than the LR calculation which has a more continuous band of RMS throughout the shear layer. This is also an indication that the HR noise predictions will contain higher frequency content, because each shock

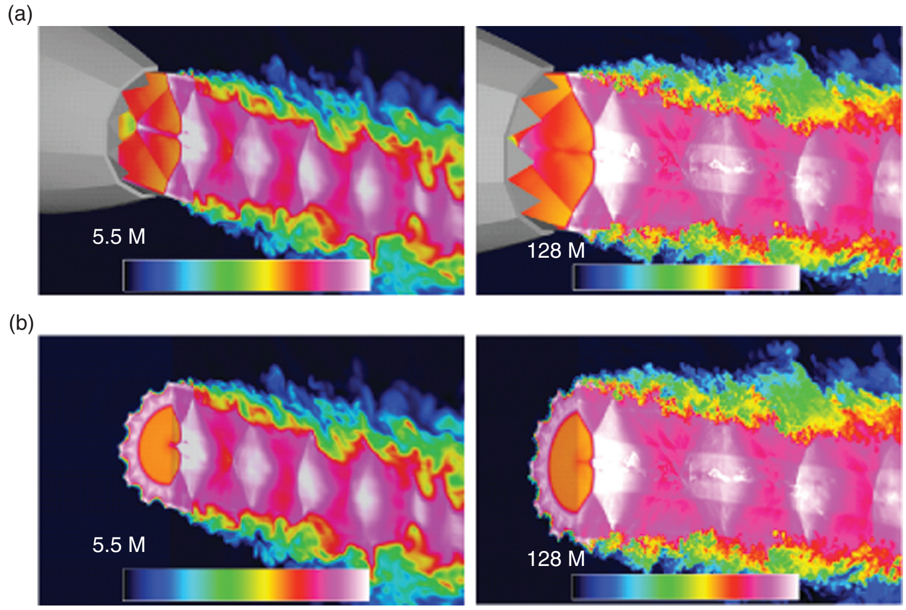

Figure 27: *Instantaneous Temperature Contours for Chevron, LR (5.5 M) vs HR (128 M) (a) z-Cut at Centerline (b) z-cut with x-cut at ~ 0.2 DJ.*

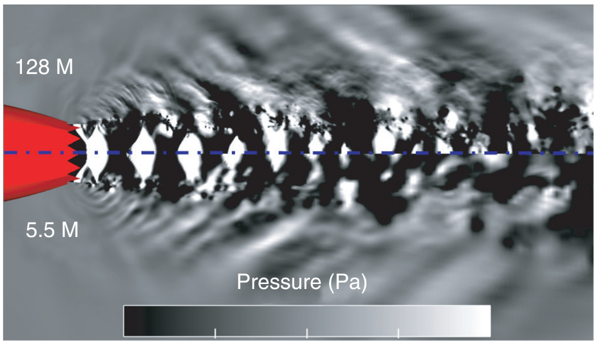

Figure 28: *Instantaneous Pressure. Fine vs. Coarse LES.*

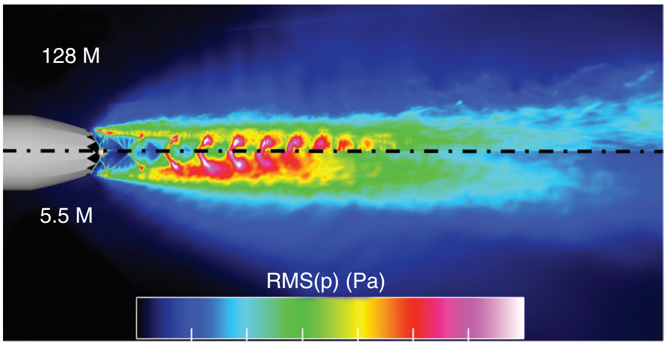

Figure 29: *RMS Pressure, Fine vs Coarse LES.*

cell is producing these high amplitude peaks in the RMS contours. There are also more peaks resolved further downstream than the LR calculation.

The far-field narrowband spectra levels are compared in Figure 30 for both resolutions of the chevron jet, in the upstream, transverse, and downstream directions. In the upstream direction it is clear that the HR calculation increases the noise levels throughout the entire frequency range and especially at levels above the BBSAN peak. This is attributed to the increased high wavenumber resolution especially in the shock cell region. Due to limited sampling time, no conclusions can be made about the lower frequencies because they are under-resolved. In the transverse

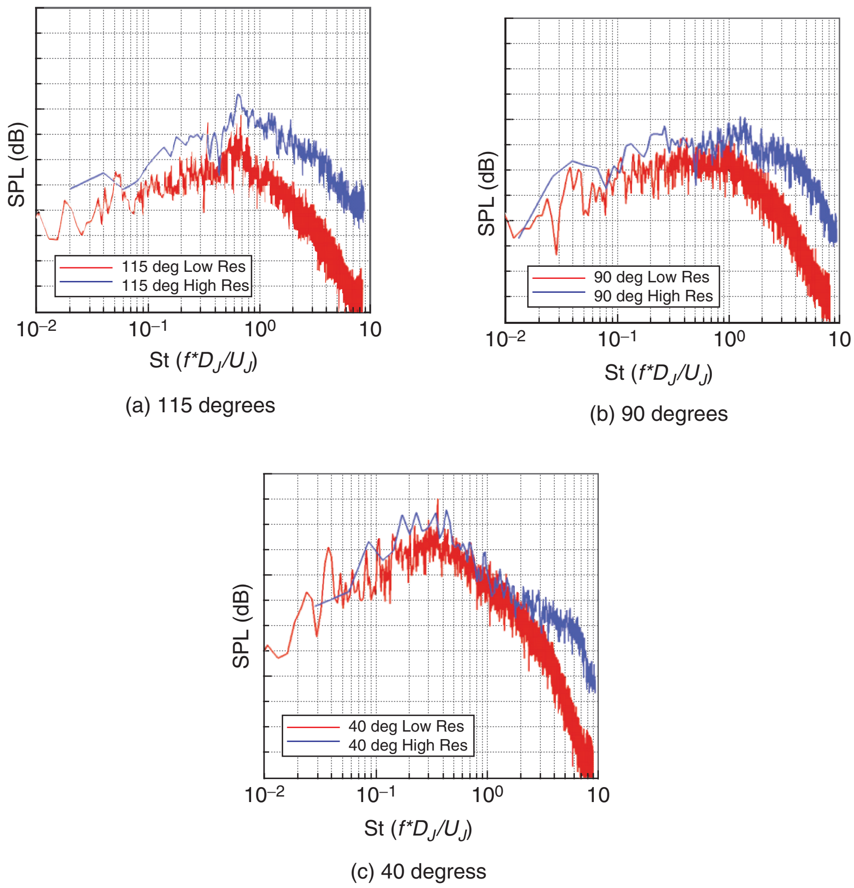

Figure 30: Coarse vs. Fine LES/FW-H Noise Predictions for Hot Military Gas Turbine Engine with Chevrons.

direction, the levels also increase above the BBSAN peak. In the downstream direction where the peak noise levels exist due to Mach wave radiation, the HR grid only appears to increase the high frequency content above a Strouhal number of around 2–3 which is well beyond the peak frequency of interest in this direction. Although the high frequency resolution for the two cases is difficult to identify, it is somewhere around St = 3 for the LR grid and St = 7 for the HR grid.

The LES/FW-H method has been applied to a hot jet with chevrons and is shown to be sensitive enough to predict the change in noise from noise reduction concepts. Additionally, the 128 million high resolution calculation was performed for the chevron jet and high frequency noise content is recovered, as expected. However, for the peak Mach wave radiation noise in the downstream direction, the lower 5.5 million cell grids appear to be sufficient.

4.3. HOT, OVER-EXPANDED TWIN-JET IMPINGING ON A JET BLAST DEFLECTOR

The Jet Blast Deflector (JBD) geometry and configuration was designed to duplicate the experimental setup at the NCPA facility. Figure 31(a) is a picture of the tenth scale twin-jet nozzle in the NCPA facility with the JBD in place. The vent hood at the top of the figure is an experimental source of error when comparing the LES/FW-H results with the experimental measurements. This hood was used to protect the anechoic foam at the top of the facility and may contaminate the near-field microphone measurements due to structural vibrations. The angle of the jet axis to the ground was set to 0.5 degrees nose-up. The JBD is inclined at an angle of 50 degrees from the deck. For this laboratory model simulation, the JBD was 43.2 inches wide and 16.8 inches long, which corresponds to a total height of 12.84 inches above the deck

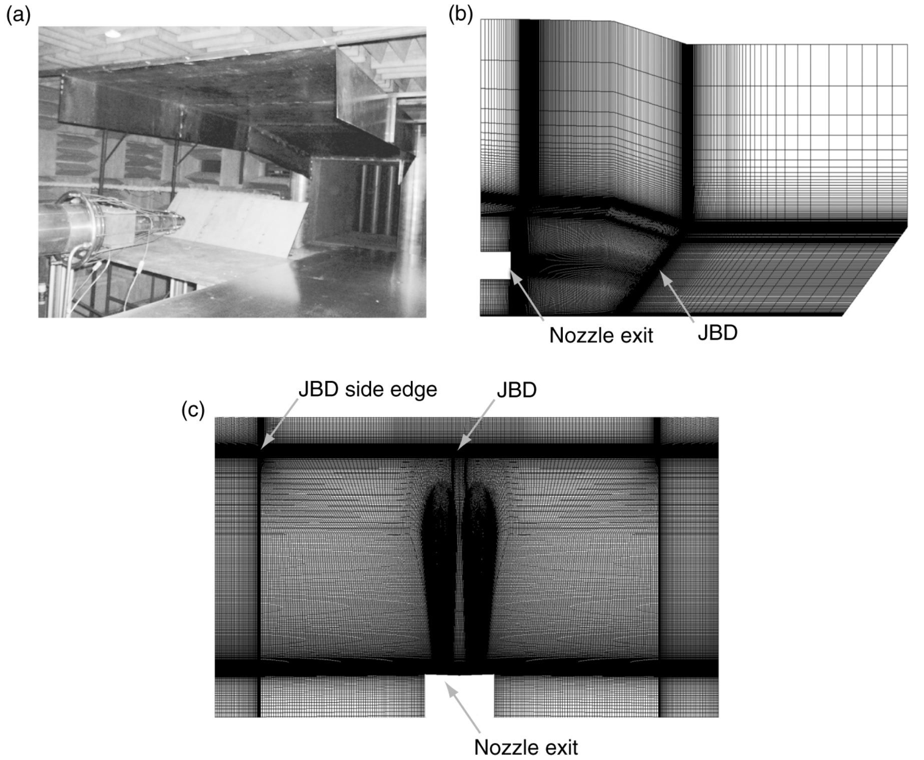

Figure 31: Twin jet impinging on Jet Blast Deflector (a) Experimental setup at NCPA (b) Side view of LES grid topology (b) Top view of LES grid topology.

surface. The tip of the twin jet nozzles was placed 18.3 inches in front of the hinge point on the JBD.

The side and top topologies for the 41 million cell JBD grid can be seen in Figure 31(b) and (c), respectively. The grid begins about 3 D_J upstream of the nozzle exit plane where freestream conditions are enforced. At the nozzle exit we enforce a fixed-flux type boundary condition from a precursor RANS simulation of the internal nozzle. Although with the tools currently available a soft-interface hybrid RANS/LES simulation is possible, this calculation was performed before these tools were ready for use. The grids are gently stretched between the nozzle exit plane and the JBD surface. Similar wall normal resolution exists on the JBD surface compared to the nozzle exit resolution; however the resolution on the ground plane is relaxed to alleviate grid cell count. Fairly aggressive buffer zone stretching exists above, behind, and to the sides of the JBD to minimize solution contamination from boundaries. A large area of the ground plane surrounding the elevated JBD is included in the LES. No NBI are used but will be in future calculations to simplify grid topologies and make more efficient use of the computational grid.

Well resolved vortical structures can be seen in the instantaneous contours of Figure 32(a) and (b) in proximity to the side and top JBD edges. Also, intense Mach wave radiation can be seen along with impinging tones that are generated by the jet exhaust impinging on the JBD surface, in addition to scattering from the JBD edges. Figure 33(a) is a top and side view schematic of the microphone locations in the NCPA experiment. An iso-surface of Mach number illustrates the exhaust impinging on the JBD. The microphones are located at a height above the deck surface equivalent to four feet at full scale. A “tight” and “loose” FW-H surface were used for noise predictions, illustrated in Figure 33(b) and (c), respectively. The loose surface is expected to lack high

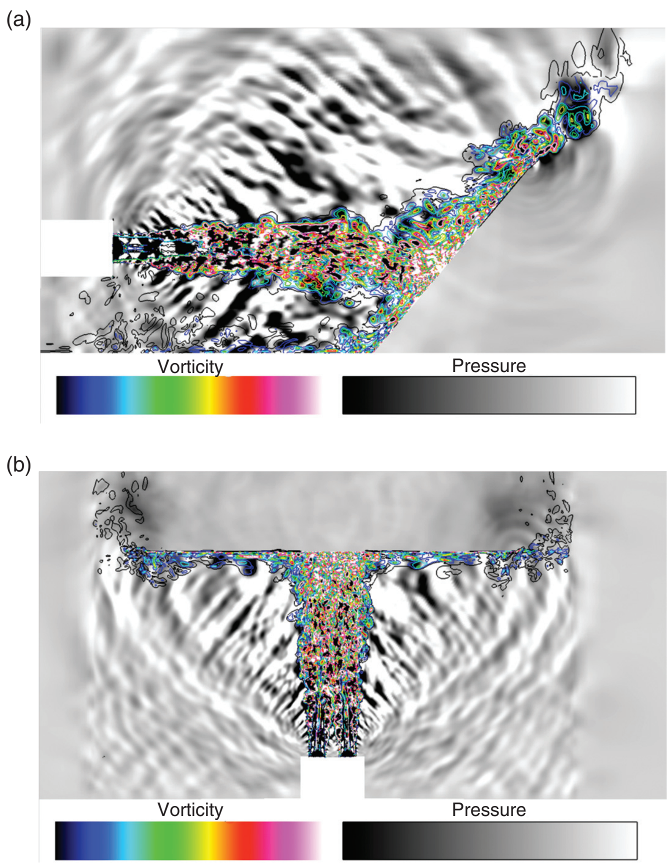

Figure 32: *Instantaneous LES pressure and vorticity contours for twin-jet JBD (a) Side view through center of right nozzle (b) Top view.*

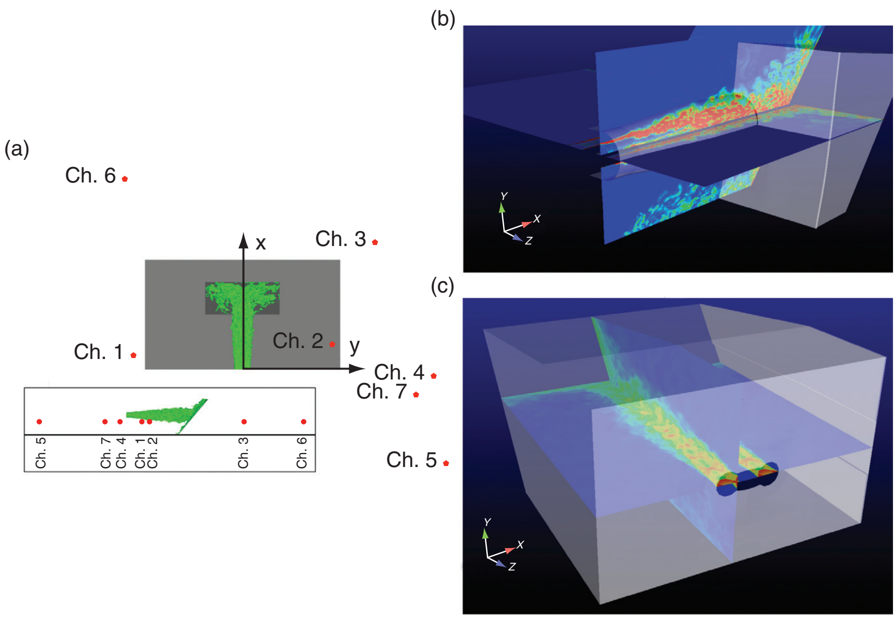

Figure 33: *(a) Microphone layout for NCPA experiment (b) Tight FW-H surface (c) Loose FW-H surface.*

frequency content due to the coarser grid spacing at the boundaries of the LES domains, relative to the tighter surface located close to the shear layer. OASPL comparisons for all microphone locations are shown in Figure 34(a) for the NCPA experiment and both FW-H surfaces. The LES/FW-H method is capturing the relative OASPL levels between the microphone locations well, but between 4 and 5 dB lower than the experiment. Shown in Figure 34(b) and

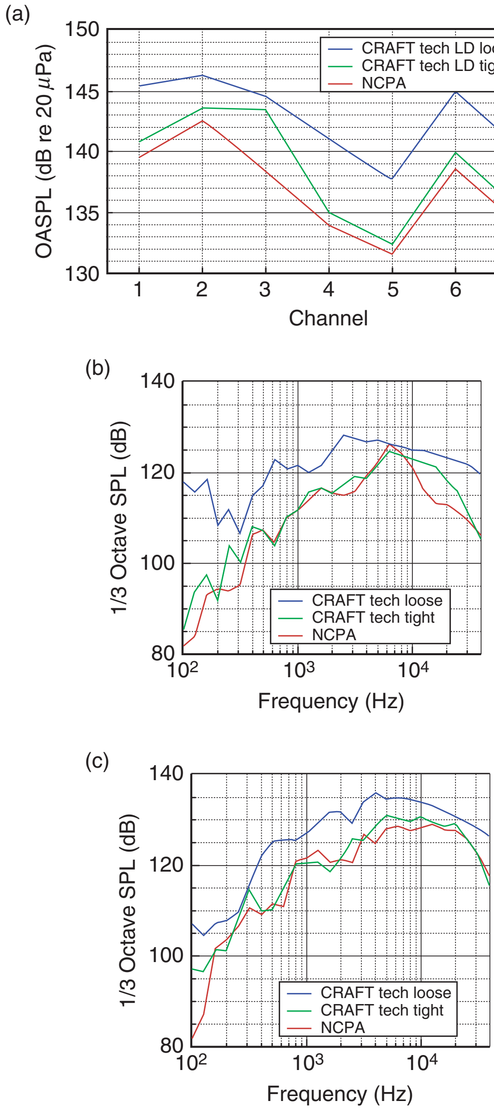

Figure 34: Far-field noise predictions for twin-jet impinging on JBD (a) OASPL compared with measurements and spectra for (b) Channel 5 (c) Channel 6.

(c) are 1/3 Octave SPL comparisons for microphones 5 and 6, respectively. There is clearly an under-prediction of sound relative to the NCPA experimental data. Note that these calculations were performed without the LDDRK time integrator and also did not include NBI. In the future, the LDDRK scheme will be used in this case as well as NBI to improve grid efficiency. More experimental datasets and careful examination of the FW-H noise results are required for full validation, but the LES/FW-H methodology has proven to handle this complex configuration.

4.4. HIGH ASPECT RATIO RECTANGULAR JETS

High aspect ratio nozzles are often considered for future aircraft propulsion systems. They have the ability to produce similar thrust while increasing stealth and improving aerodynamic efficiency on the installed aircraft [31]. Also, embedding the propulsion systems can lead to reduced sonic boom signatures [33]. It is essential for the current tools to be capable of predicting the noise for these types of nozzles and not limited to round nozzles. The final application in this paper is a 4:1 rectangular nozzle, with and without a

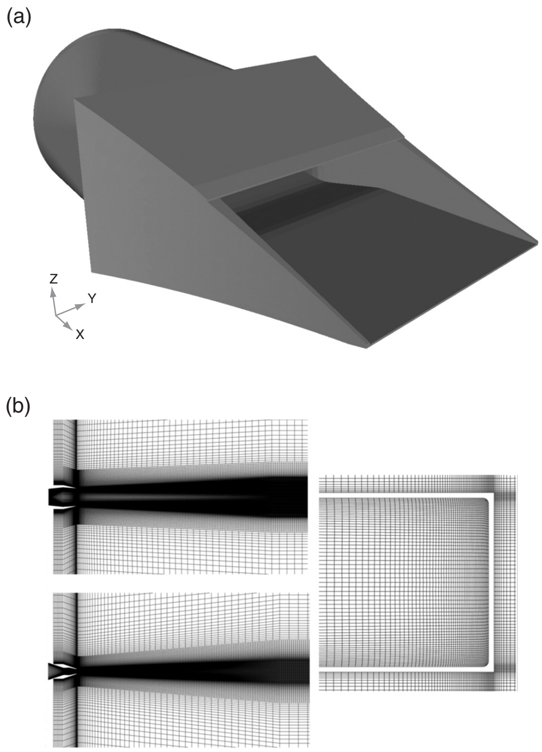

Figure 35: (a) Nozzle geometry for NA4B2 and (b) LES grid topology for baseline 4:1 nozzle.

bevel. The bevel is a noise reduction concept that has the potential to alter the directivity of the noise and possibly shield noise from reaching undesirable locations, such as a community around an airport.

The Extensible Rectangular Nozzle (ERN) model system was developed by the NASA Supersonics Project [32]. The initial goal of the testing was to determine whether or not rectangular nozzles have the potential for noise reduction. To aid this study, CRAFT Tech has performed high resolution RANS/LES calculations using the DDES implementation. The 4:1 rectangular baseline nozzle was simulated and also with a bevel extending 2.8 nozzle heights from the long edge, denoted NA4B2. Setpoint 7 was run for both nozzles which is cold (unheated) with an acoustic Mach number of 0.9. Figure 35(a) is a view of the NA4B2 nozzle geometry, and the LES grid topology generated for the baseline nozzle is shown in Figure 35(b). The fillets along the inner nozzle edges are resolved.

Flowfield solutions for the baseline and beveled nozzles are shown in Figure 36 and Figure 37. A qualitative difference in the vorticity and acoustic field can be seen when the nozzle is beveled. Close to the beveled upper nozzle lip in Figure 37(b), a tonal source can be seen radating outward. Also, multiple tones can be seen radiating from the lower lip. A careful examination of this near-nozzle shielding and scattering is required in order to assess the effect of beveling on rectangular nozzles. In the future, quantification of the noise differences will be made by coupling the LES calculations with the FW-H acoustic solver.

5. CONCLUDING REMARKS

In this paper we have described realistic jet noise predictions using a coupled Large Eddy LES and FW-H equation approach. For the LES calculations we use a structured grid Navier Stokes solver, CRAFT CFD®, which has low dissipation and higher order spatiotemporal numerics as well as non-contiguous block interfacing capability

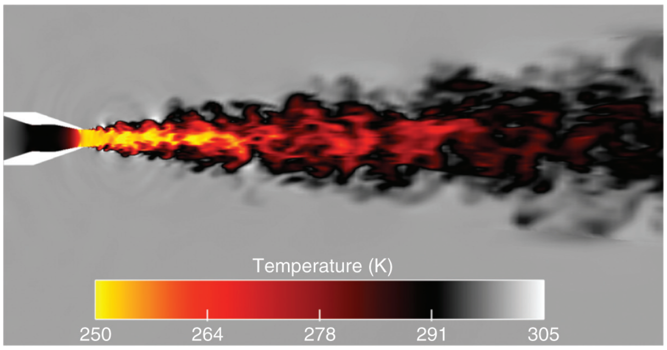

(a) Baseline 4:1

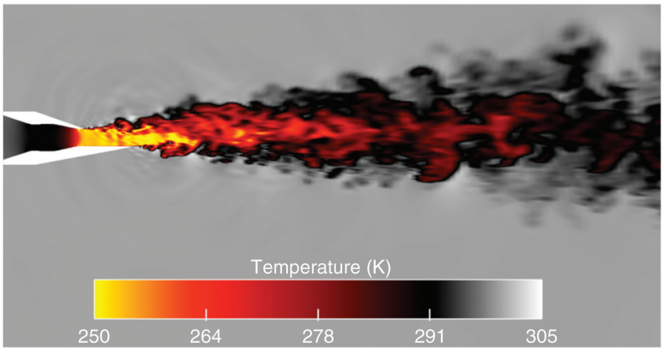

(b) Beveled 4:1

Figure 36: *Instantaneous temperature contours for (a) Baseline and (b) Beveled 4:1 jet.*

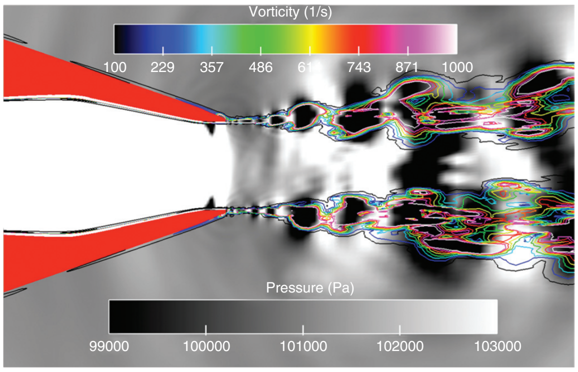

(a) Baseline 4:1

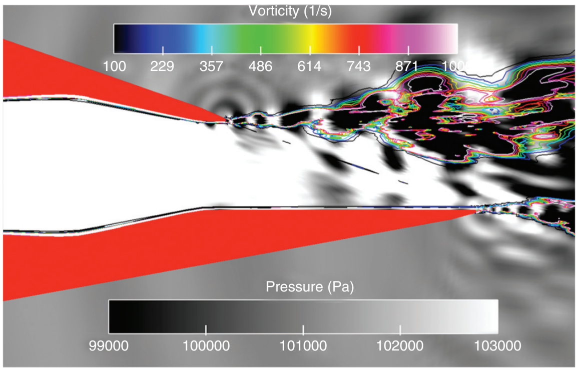

(b) Beveled 4:1

Figure 37: *Instantaneous pressure and vorticity contours for (a) Baseline and (b) Beveled 4:1 jet.*

to reduce grid sizes. The far-field noise is solved with the FW-H equation. Four demonstration cases were shown, each of which are a state of the art application of the methodology.

The first case is an LES and far-field noise prediction for a corrugated faceted nozzle using CRAFT Tech optimized lobes, designed for reduced noise with no thrust penalty. Excellent far-field noise agreement with experimental measurements at NCPA is shown. The second case applies the tools to the prediction of noise from a hot military gas turbine engine exhaust with and without chevrons. The ability of the LES to capture the effect of the chevrons on the flowfield and associated far-field noise is investigated. The chevrons are shown to reduce the far-field noise between 1 and 2 dB at all angles to the jet and as much as 4 dB downstream. The third case is a twin heated jet impinging on a jet blast deflector. The entire jet and impinging region is enclosed with a FW-H surface and noise predictions are compared with NCPA experimental measurements at various representative sailor locations on the ship deck. The last application are two high aspect ratio rectangular jet calculations, one with and one without a bevel. Again, NBI are used in order to reduce grid requirements while maintaining the benefit of a structured grid solver. All of the above applications use hybrid RANS/LES interfacing to solve the entire flowfield, blending RANS solutions of the internal nozzle with highly resolved LES of the exhaust. Typical run times range from a few days for the coarser grids to two weeks for the high-resolution chevron calculation.

The future promises more complex problems that will challenge these LES/FW-H tools even further. Generating a clean and efficient grid is a time-consuming and challenging task. The codes themselves are proving capable of handling a wide variety of flow configurations, but regardless of the selected numerical schemes, there is no substitute for a quality grid. These tools shown here are useful for turbulence driven problems where resolving a wide range of scales is critical for predicting the correct noise. Careful comparison of LES flowfield statistics need to be made with experimental measurements, because turbulence in the shear layer directly effects the far-field noise predictions. When enough confidence is gained through full scale testing and validation, the LES/FW-H methodology can be applied to improve the design of realistic configurations and not merely reproducing experimental laboratory measurements.

ACKNOWLEDGEMENTS

Parts of this work were sponsored by NAVAIR Propulsion and Power Awards and funding from University of Mississippi's National Center for Physical Acoustics.

REFERENCES

[1] Lyrintzis, Anastasios S., and Gregory A. Blaisdell. "Jet Noise Predictions Using Large Eddy Simulations." *2nd International Conference on Fluid Mechanics and Heat & Mass Transfer*. 2011.

[2] Bodony, D. J. and Lele, S. K., "Current Status of Jet Noise Predictions Using Large-Eddy Simulation," *AIAA Journal* **46**:2, Feb. 2008.

[3] Shur, M.L., Spalart, R. P., Strelets, M. K., and Garbaruk, A. V., "Further Steps in LES-Based Noise Prediction for Complex Jets," *Presented at the 44th AIAA Aerospace Sciences Meeting and Exhibit*, AIAA 2006-0485, 2006.

[4] Bodony, D. J., "The prediction and understanding of jet noise," *Center for Turbulence Research Annual Research Briefs*, 2005.

[5] Spalart, P. R., Shur, M. L., Strelets, M. K., and Travin, A., "Sensitivity of Landing-Gear Noise Predictions by Large-Eddy Simulation to

Numerics and Resolution," 50th AIAA Aerospace Sciences Meeting, Jan. 2012.

[6] Uzun A., Blaisdell G. A., and Lyrintzis, A. S. "Coupling of Integral Acoustics Methods with LES for Jet Noise Prediction," *Journal of Aeroacoustics*, Vol. 3, No. 4, Oct. 2004, pp. 297–346.

[7] Kim, J., and Choi, H., "Large eddy simulation of a circular jet; effect of inflow conditions on the near field," *J. Fluid Mech.* Vol. 620 pp. 383–411, 2009.

[8] Sinha, N., Kenzakowski, D., Ungewitter, R., Dash, S., and Seiner, J., 2008. "Computational and Experimental Investigations of Jet Noise Reduction Concepts for Low Bypass Ratio Military Gas Turbine Engines". ASME Turbo Expo 2008, ASME Paper GT 2008-50091.

[9] Sinha, N., Erwin, J. P., Kannepalli, C., and Arunajatesan, S., "LES Predictions of Noise Emissions from a Low-Bypass Ratio Military Gas Turbine Engine," ASME Turbo Expo 2010, ASME Paper GT 2010-22191.

[10] Erwin, J. P. and Sinha, N., "Near and Far-field Investigations of Supersonic Jet Noise Predictions using a coupled LES and FW-H equation approach," ASME Turbo Expo 2011, ASME Paper GT 2011-45210.

[11] Erwin, J. P., Sinha, N., and Rodebaugh, G. P., "Large Eddy Simulations of Supersonic Impinging Jets," *Journal of Engineering for Gas Turbines and Power*, Vol. 134 No. 121201, Dec. 2012.

[12] Kannepalli, C., Arunajatesan, S., and Dash, S., "RANS/LES methodology for supersonic transverse jet interactions with approach flow," AIAA 2002-1139.

[13] Calhoon, W., Kannepalli, C., Arunajatesan S., and Dash, S., "Analysis of Scalar Fluctuations at High Convective Mach Numbers," AIAA 2002-1087.

[14] Tam, C. K. W. and Dong, Z., "Radiation and outflow boundary conditions for direct computation of acoustic and flow disturbances in a nonuniform mean flow," *Journal of Computational Acoustics*, Vol. 4 No. 2, pp. 175–201, 1996.

[15] Bogey, C. and Bailly, C., "Three-dimensional non-reflective boundary conditions for acoustic simulations: far field formulation and validation test cases," *Acta Acustica United with Acustica,* Vol. 88 pp. 463–471, 2002.

[16] Brinckman, K. W., Calhoon, W.H., J., and Dash, S. M., "Scalar Fluctuation Modeling for High-Speed Aeropropulsive Flows," *AIAA Journal*, Vol. 45, No. 5, May 2007, pp. 1036–1046.

[17] Brinckman, K. W. and Dash, S., "Improved Methodology For RANS Modeling Of High-Speed Turbulent Scalar Mixing," 50th AIAA Aerospace Sciences Meeting, AIAA 2012-0567, Jan. 2012.

[18] Arunajatesan, S., and Sinha, N., "Hybrid RANS/LES Modeling for Cavity Aeroacoustics Predictions," *Journal of Aeroacoustics*, Vol. 2, No. 1, pp. 65–93, 2003.

[19] Fröhlich, J. and von Terzi, D., "Hybrid LES/RANS methods for the simulation of turbulent flows," Progress in Aerospace Sciences, Vol. 44, July 2008, pp. 349–377.

[20] Spalart, P. R., "Detached-Eddy Simulation," Annual Review of Fluid Mechanics, Vol. 41, Jan. 2009, pp. 181–202.

[21] Spalart, P. R., Deck, S., Shur, M. L., Squires, K. D., Strelets, M. K., and Travin, A., "A New Version of Detached-eddy Simulation, Resistant to Ambiguous Grid Densities," Theoretical and Computational Fluid Dynamics, Vol. 20, July 2006, pp. 181–195.

[22] Rodebaugh, G. P., Brinckman, K. W., and Dash, S. M., "DDES of Aeropropulsive Flows Based on an Extended *k-e* RANS Model," *Presented at the 51st AIAA-2013-0393 Aerospace Sciences Meeting*, Grapevine, Texas, January 2013.

[23] Hu, F. Q., Hussaini, M. Y. and Manthey, J.,

"Low-dissipation and -dispersion runge-kutta schemes for computational aeroacoustics," NASA ICASE Report No. 94–102, December 1994.

[24] Benek, J. A., Steger, J.L., Dougherty, F.C., and Buning, P.G., "Chimera. A Grid-Embedding Technique," Final Report for Period November 1, 1980 - Oct. 1, 1985, Arnold Engineering Development Center, AEDC-TR-85-64, April 1986.

[25] Farassat, F. NASA/TM-2007-214853, "Derivation of Formulations 1 and 1A of Farassat", Langley Research Center, Hampton, VA, 2007.

[26] Brentner, K. S. and Farassat, F., "An analytical comparison of the acoustic analogy and kirchhoff formulation for moving surfaces," *53rd Annual American Helicopter Society Forum*, *AIAA Journal* Vol. 36 No. 8, August 1998, pp. 1379–1386.

[27] Seiner, J. M. and Norum, T. D., "Experiments on shock associated noise of supersonic jets," AIAA 1979-1526.

[28] Freund, J. B., "Noise sources in a low-Reynolds-number turbulent jet at Mach 0.9," *Journal of Fluid Mechanics*, Vol. 438, 2001, pp. 277–305.

[29] Spalart, P. R. and Shur, M. L., "Variants of the Ffowcs Williams-Hawkings equation and their coupling with simulations of hot jets," *International Journal of Aeroacoustics*, Vol. 8 No. 5, 2009, pp 477–492.

[30] Lyrintzis, A. S., "Integral Acoustics Methods: From the (CFD) Near- Field to the (Acoustic) Far-field," *International Journal of Aeroacoustics* Vol. 2, No. 2, 2003 pp. 95–128.

[31] Nichols, J., Ham, F., Lele, S., and Bridges, J., "Aeroacoustics of a supersonic rectangular jet: Experiments and LES predictions," AIAA 2012-0678.

[32] Bridges, J., "ERN11 Analysis", NASA Technical Document, 26 Jan 2011.

[33] Bridges, J., "Noise of Embedded High Aspect Ratio Nozzles," Presented at the 2011 Technical Conference for the Fundamental Aeronautics Program Supersonics Project. Cleveland, OH, March 2011.

NOTTINGHAM NIGHTCLUB FINED £67,000 FOR NOISE, LOSES LICENCE

The operators of Nottingham Nightclub F&G have been fined more than £67,000 for making too much noise - despite several warnings to quieten down. Unique Nightclub Ltd, which runs F&G, was convicted of 16 breaches of a noise abatement notice at Nottingham Magistrates court. District Judge Justice Pyle fined the company £4,000 for each offence plus costs. The total bill added up to £67,872.69. Community Protection had been investigating complaints from a number of residents about loud music coming from the club and on January 10 this year, a noise abatement notice was served on Unique Nightclub Ltd, requiring them to stop causing a noise nuisance. Despite both verbal and written warnings to the club's operators, complaints about the noise continued to be received. Lorraine Raynor, Head of Environmental Health & Trading Standards for Community Protection said: "Officers collated evidence of the breaches using digital recording equipment installed in the complainants' properties. The assessment of these recordings, witness statements of officers and victim impact statements provided by a number of residents provided the evidence upon which the prosecution was based." Over the last six months, three warrants were applied for and our bailiffs entered the premises and seized music equipment on two occasions," said Mrs Raynor. "Following this, new equipment was obtained and the noise nuisance continued." In sentencing, the Judge stated that he had found that the breaches were deliberate and persistent and that the effect of the statutory noise nuisance on the residents was real and constant, affecting both their sleep and ability to do their jobs. The club's licence was also revoked at a hearing of Nottingham City Council's licensing authority.

SOMETHING NEW TO COMPLAIN ABOUT

The growing popularity of skydiving as a leisure activity has given rise to new protest movement - among residents enraged by the sound of circling planes. Anger is building across the UK at so-called "nuisance sky-diving" - in particular the noise made by circling aircraft as they prepare to release their adrenalin-junkie passengers. The number of people skydiving at the UK's 26 specialist clubs is higher than ever, according to the British Parachute Association, rising from 188,000 in 1998 to 250,000 in 2012. An estimated half of all skydivers throw themselves out of planes in the name of charity, but noise campaigners are now asking them to find less noisy ways of raising money for good causes. Resident groups in Wiltshire, Gloucestershire, Oxfordshire and Cumbria are among those campaigning about the noise caused by skydiving. Members of the Residents Against Redlands campaign claim that skydivers taking off from the Redlands Airfield in Wanborough, East Swindon, generate more than 12 hours of noise disturbance every Friday, Saturday and Sunday. Kay Lacey, who moved to the area before skydiving from light aircraft began in 2000, said: "They are breaking maximum UK noise levels. Eighty decibels is at the top end of what's considered loud enough to cause distress, but the skydiving planes reach 100. It's a hellish droning sound which causes vibrations inside houses as well. When the Civil Aviation Authority grants licences they don't test aircraft noise at full throttle, which is what planes fly at." The residents have collected almost 1,000 signatures on a petition calling for the noisiest plane model - the Gippsland G8 - to be grounded, but the airfield has so far declined to act.